

Suppression of Near-Fermi Level Electronic States at the Interface in a LaNiO₃/SrTiO₃ Superlattice

A. M. Kaiser,^{1,2,3} A. X. Gray,^{1,2} G. Conti,^{1,2} J. Son,⁴ A. Greer,^{1,2} A. Perona,^{1,2} A. Rattanachata,^{1,2} A. Y. Saw,^{1,2} A. Bostwick,⁵ S. Yang,⁶ S.-H. Yang,⁷ E. M. Gullikson,⁶ J. B. Kortright,² S. Stemmer,⁴ and C. S. Fadley^{1,2}

¹Department of Physics, University of California, Davis, California 95616, USA

²Materials Sciences Division, Lawrence Berkeley National Laboratory, Berkeley, California 94720, USA

³Peter-Grünberg-Institut PGI-6, Forschungszentrum Jülich, 52425 Jülich, Germany

⁴Materials Department, University of California, Santa Barbara, California 93106, USA

⁵Advanced Light Source, Lawrence Berkeley National Laboratory, Berkeley, California 94720, USA

⁶Center for X-Ray Optics, Lawrence Berkeley National Laboratory, Berkeley, California 94720, USA

⁷IBM Almaden Research Center, San Jose, California 95120, USA

(Received 2 July 2011; published 9 September 2011)

Standing-wave-excited photoemission is used to study a SrTiO₃/LaNiO₃ superlattice. Rocking curves of core-level and valence band spectra are used to derive layer-resolved spectral functions, revealing a suppression of electronic states near the Fermi level in the multilayer as compared to bulk LaNiO₃. Further analysis shows that the suppression of these states is not homogeneously distributed over the LaNiO₃ layers but is more pronounced near the interfaces. Possible origins of this effect and its relationship to a previously observed metal-insulator-transition in ultrathin LaNiO₃ films are discussed.

DOI: 10.1103/PhysRevLett.107.116402

PACS numbers: 71.30.+h, 79.60.Jv

During the past decade, multilayer oxide heterostructures have stimulated great interest due to the fact that they can possess functional properties not present in the associated bulk materials or in single layers [1,2]. In particular, oxide heterostructures containing thin LaNiO₃ (LNO) layers have recently become an active research topic due to the possibility of controlling the electronic properties by adjusting the layer thicknesses and the companion oxides: In contrast to its sister compounds in the RNiO₃ (R = rare earth) series, bulk LNO is a Fermi liquid and remains metallic at all temperatures [3]. In heterostructures or superlattices of LNO, these properties can change drastically. For example, recent studies show that ultrathin films of LNO undergo a metal-insulator transition (MIT) [4,5], while superlattices of LNO with SrTiO₃ (STO) show an increase of conductivity [6]. Theoretical calculations also predict the manifestation of superconductivity in superlattices comprising single layers of LNO [7,8].

As many of these effects are considered to be related to interfacial properties, it is desirable to employ an experimental method allowing for depth-resolved studies of the electronic structure. One such method is standing-wave excited x-ray photoemission spectroscopy (SWXPS), which has proven to be a reliable tool for nondestructively probing the electronic structure of buried films and interfaces [9,10]. This technique needs a sample that is, or is grown on, a periodic multilayer mirror, and it exploits the fact that when the Bragg condition for the mirror is satisfied, a standing wave with the same periodicity as the multilayer is created within the sample. Consequently, the photoemission yield is locally enhanced at the maxima of the standing wave. By slightly detuning the incidence

angle off the Bragg resonance, the phase of the standing wave can be shifted by $\sim 180^\circ$. Thus, by collecting photoelectron spectra at different angles around the Bragg resonance and comparing the experimental rocking curves with x-ray optical calculations, a depth profile of the electronic states can be extracted.

We have used SWXPS to study an epitaxial superlattice consisting of 10 bilayers of 4 unit cells (u.c.) thick LNO and 3 u.c. thick STO grown on a (001) (LaAlO₃)_{0.3} × (Sr₂AlTaO₃)_{0.7} substrate by rf magnetron sputtering. X-ray diffractometry and high-resolution transmission electron microscopy confirmed epitaxial growth with the superlattice coherently strained to the (LaAlO₃)_{0.3}(Sr₂AlTaO₃)_{0.7} substrate, as well as the sharpness of the interfaces, while electrical measurements revealed metallicity for the superlattice [5,6].

The experiments have been carried out at room temperature at Beam line 7.0.1 of the Advanced Light Source in a ultrahigh vacuum chamber equipped with a hemispherical electron analyzer (VG Scienta R4000). The angle between incident x rays and the direction of the detector was set to 60° . A photon energy of 833.2 eV just below the La $3d_{5/2}$ resonance was used to enhance reflectivity [10]. The experimental resolution at this energy was 300 meV. By measuring x-ray absorption spectra around this energy and via the Kramers-Kronig transformation, the complex index of refraction in that energy range was calculated. Via separate x-ray reflectometry measurements, the Bragg condition for the multilayer periodicity of $d_{ML} = 27.3 \text{ \AA}$ was found to be satisfied for an incidence angle of $\theta = 15.9^\circ$, as measured from the sample surface, and the FWHM of the superlattice reflectivity peak was 1.6° , in good

agreement with x-ray optical simulations carried out with the YXRO program [11]. Photoemission survey spectra from 0 to 600 eV binding energy revealed peaks from all the expected elements with the only contaminant being a surface layer of carbon- and presumably also oxygen-containing adsorbates that we designate as CO_x , the thickness of which has been estimated to be about 9 Å by model calculations [12]. Survey spectra before and after the standing-wave experiments (~ 12 h) showed an increase of the C intensity during the illumination by the x-ray beam; this is reasonable as STO surfaces are known to have a strong propensity for adsorption and formation of carbon hydroxyl layers [13,14].

For the SWXPS experiments, the incidence angle was varied from 13.0° to 17.4° in 0.1° increments. For each constituent element of the superlattice the strongest core level was chosen (O $1s$, Ti $2p_{3/2}$, Sr $3d_{5/2}$, C $1s$, La $4d_{5/2}$, and Ni $3p$), and for each angular step spectra of these core levels and the valence bands were collected. O $1s$ consists of three shifted components at binding energies of 528.1, 529.5, and 530.3 eV with the peak at 529.5 eV strongly dominating the measured spectra and verified below to be O as a constituent of STO.

The peak areas of each peak were determined by subtracting a Shirley-background [15] and peak fitting using Voigt profiles. Figure 1(a) compiles the resulting core-level rocking curves showing the angular behavior of the peak areas together with a x-ray optical calculation [11]. The different rocking curves are normalized to the average intensity over the angular range and offset for clarity. For this analysis, tabulated optical properties [16] were used for the STO and calculated values allowing for the resonant energy for LNO, as described above.

A first set of x-ray optical calculations using the nominal sample parameters of 10 bilayers of STO (3 u.c. = 11.7 Å) and LNO (4 u.c. = 15.6 Å) did not yield satisfactory agreement with all of the experimental rocking curves. This agreement could be markedly improved by adjusting only the thickness of the topmost STO layer downward slightly to 9 Å; the thickness of the adventitious CO_x layer was set to the previously estimated 9 Å. Excellent agreement was then found by modeling the top and bottom interfaces via a linear interdiffusion with different parameters. The LNO on STO interfaces were found to be very sharp, with only a 1 Å thick interdiffusion, but the STO on LNO interfaces were somewhat thicker at 3 Å. Similar effects have been reported for various superlattices due to differences in the surface free energy [17]. As shown in Fig. 1(a), all of the features of the experimental rocking curves are well reproduced by the simulations using this set of parameters. The different components of the O $1s$ peak were found to exhibit different rocking curves of clear STO type for the strongest peak at 529.5 eV and LNO type for the one at 528.1 eV. In fact, we find excellent agreement by simulating the rocking curves for O atoms from STO (529.5 eV) and LNO (528.1 eV)

separately. The higher binding energy and much weaker component at 530.3 eV expected to be related to the CO_x surface layer did not show any clear rocking curve.

For some of these curves, particularly C $1s$ and Ni $3p$, the shapes of the rocking curves are correctly predicted, but the theoretical magnitudes of the modulation are consistently lower than experiment by a factor of 2. This discrepancy may be due to several factors such as an inaccurate fitting of the Ni $3p$ peaks because of their overlap with the Ti $3s$ peak, an increase of the thickness of the CO_x layer during the measurements, an inhomogeneous vertical distribution of the CO_x surface contaminant not included in the x-ray optical simulations, and/or inaccurate knowledge of the x-ray optical constants of LNO and STO, particularly in the interface region [10]. However, for the whole set of rocking curves, we find excellent agreement of the positions of maxima and minima and thus estimate that the thickness

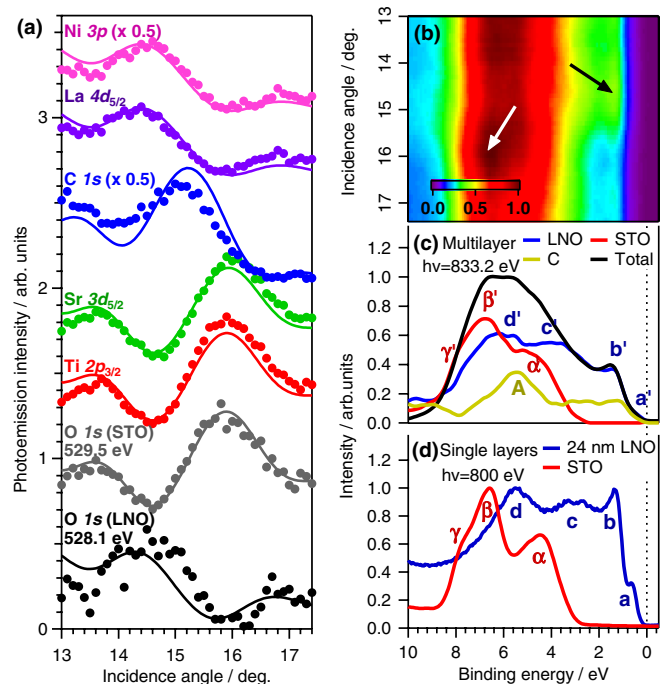


FIG. 1 (color online). (a) Experimental rocking curves (round markers) for all relevant core levels with best theoretical fits. The different rocking curves are normalized to the average intensity over the angular range of interest and offset for clarity. The experimental curves for Ni $3p$ and C $1s$ are multiplied by the values indicated for a better agreement of theory and experiment. (b) Intensity map of the valence band region for different incidence angles with the color scale corresponding to the photoemission yield. Two characteristic maxima split by 1.4° are marked by black and white arrows, respectively. (c) Total valence band (black curve) of the STO/LNO multilayer with deconvoluted components showing the characteristic angular behavior of LNO (blue curve), STO (red curve), and C (brown curve). (d) Valence bands of a STO single crystal (red curve) and 24 nm LNO on STO (blue curve). Characteristic features are labeled by lowercase Latin letters for LNO, Greek letters for STO, and uppercase Latin letters for C.

profile on which our model is based describes the real sample with an error of less than $\pm 2 \text{ \AA}$. Furthermore, the fact that we do not observe any significant shift or difference between core-level rocking curves from the same layer shows that no segregation of one element relative to another element occurs at the STO/LNO interfaces.

The valence band (VB) spectrum shown in Fig. 1(c), integrated over the full angular range, contains contributions from different electronic states of the constituent atoms. Because of this superposition of spectral components, it is not feasible to analyze the valence band region by using the same procedure as the core levels. However, if we look in detail at the full set of VB spectra in Fig. 1(b), we note markedly different angular behavior for different spectral regions. For example, it is obvious that maxima occur at different incidence angles, as marked by the arrows in Fig. 1(b). These two maxima are split by 1.4° , roughly corresponding to the FWHM of the rocking curve of 1.6° . When the incidence angle is varied over this range, the standing-wave field is translated by half a superlattice period. Thus, it can be concluded that these two spectral components largely originate from the two different layers in the sample. Note also that, for angles greater than about 15.8° , there is a sharp loss of intensity over binding energies from 0 to 2 eV, indicating the opening of a gap in one of the layers.

We can be somewhat more quantitative by noting that, at these energies and room temperature, the spectra are expected to be well described as a simple superposition of matrix-element-weighted projected densities of states (DOS) from the constituent atoms [18]. The measured valence band intensity map $I_{\text{VB}}(E_b, \theta)$ with binding energy E_b and incidence angle θ can then first be assumed to be a simple superposition of the valence band spectra of several layers i , $I_{\text{VB},i}(E_b)$, with a layer-dependent characteristic rocking curve $\rho_i(\theta)$. Thus, it can be written as

$$I_{\text{VB}}(E_b, \theta) = \sum_{\text{layers } i} \rho_i(\theta) I_{\text{VB},i}(E_b).$$

In general, the characteristic rocking curves ρ_i depend on the inelastic mean free path of the photoelectrons and therefore are energy-dependent [19]. However, model calculations show that this effect is negligible over the experimental range. Thus, we can further assume that the major spectral components of the valence band region show the same angular behavior as the three characteristic rocking curves found in the core-level measurements (STO: Sr $3d$, Ti $2p$; LNO: La $4d$, Ni $3p$; CO_x: C $1s$).

As a first-order approximation, we have assumed our VB data to be composed of the three components $I_{\text{LNO}}(E_b)$, $I_{\text{STO}}(E_b)$, and $I_{\text{C}}(E_b)$ with the angular characteristics $\rho_{\text{STO}}(\theta) = \rho_{\text{Ti}2p}(\theta)$, $\rho_{\text{LNO}}(\theta) = \rho_{\text{La}4d}(\theta)$, and $\rho_{\text{C}}(\theta) = \rho_{\text{C}1s}(\theta)$, respectively, as derived from the experimental data and without recourse to theory. For the deconvolution of spectral components, the VB rocking curves for each energy step have then been fitted to a linear combination of

these characteristic rocking curves by a least-square fitting routine. Finally, the fitting coefficients shown in Fig. 1(c) correspond to the layer-resolved matrix-element-weighted DOS $I_i(E_b)$.

Figure 1(d) now permits comparing the three layer-resolved VB spectra to spectra collected on a bulk STO single crystal and a 24-nm-thick LNO layer on STO, obtained with a photon energy of $h\nu = 800 \text{ eV}$. The deconvoluted spectrum ρ_{STO} for the STO in Fig. 1(c) shows excellent agreement with the one from the STO single crystal reproducing both peaks, marked with α and β , and the shoulder γ . The STO spectrum from the multilayer is slightly smeared out compared to the single crystal DOS, which may be attributed to alterations of electronic structure at the interfaces and/or to a lower crystalline quality of the thin STO layers. The STO spectrum does not show any significant spectral weight for $E_b < 2.5 \text{ eV}$ consistent with the insulating character of that layer and the valence band edge positioned at this energy.

The LNO reproduces the four prominent features a , b , c , and d present in the single film LNO experimental spectrum. However, the observed amplitudes of both samples do not match. Particularly, the features a' and b' that have been identified as the Ni e_g and t_{2g} states [20,21] are suppressed and smeared out in the multilayer sample, as compared to the single films. A similar suppression and opening of a band gap has been recently reported for thin films of LNO on LaAlO₃ or (LaAlO₃)_{0.3}(Sr₂AlTaO₃)_{0.7} [22]. Thus, we suggest that the suppression of these states is correlated to the MIT observed in thin LNO films and that the LNO layers inside the multilayer are close to a MIT.

The third spectral component showing the same angular characteristics as the C $1s$ core level contains one strong feature labeled A on a uniform background with a similar characteristics as the LNO DOS. The feature A might be related to the hybridized O $2p$ or C $1s$ levels of the CO_x contaminants or modifications of the STO surface as observed on STO samples and similar oxides [13,23]. However, if the uniform background extending up to the Fermi level was related to the CO_x adsorption on STO, it should also be observed in the STO single crystal. Here, however, we do not observe any significant contribution for $E_b < 2.5 \text{ eV}$. Thus, it is reasonable to assume that the observed spectral contribution with C $1s$ character is not a feature of the CO_x layer but rather an artifact of the fit due to a more complicated sample structure than we have assumed. In any case, it does not significantly influence our conclusions concerning the spectral components for STO and most of the components for LNO, particularly those close to the Fermi level.

A closer inspection of the experimental angular characteristics across the features labeled a' and b' associated with Ni e_g and t_{2g} shows a discrepancy with respect to the characteristics as calibrated by the La $4d$ core levels. Figure 2 shows that the angular characteristic of the energy

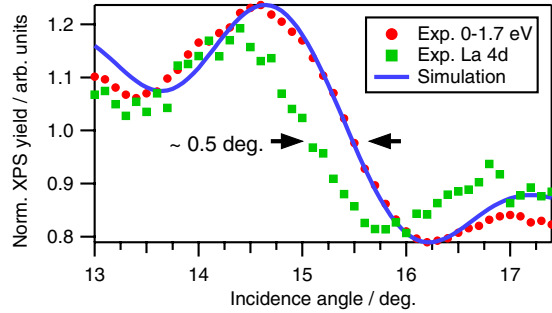


FIG. 2 (color online). Angular behavior of the spectral region near the Fermi level (red markers), the La 4d core-level characteristics for the LNO layer, and a simulated rocking curve for the inner two unit cells of the LNO layer (solid line).

region from 0 to 1.7 eV is significantly shifted relative to that for La 4d. Thus, we conclude that the DOS observed just below the Fermi level does not originate from the entire LNO layer. A much better correlation is obtained when the near- E_f spectral rocking curves are compared to a simulated rocking curve of electronic states present only in the inner two unit cells of the LNO layer with the outer unit cells adjacent to the STO layers being inactive in this spectral region. In the simulation, we have also assumed a linear 4 Å gradient in the electronic structure of these states within LNO. Thus, the discrepancy of the rocking curves in Fig. 2 suggests that the Ni e_g and t_{2g} states are preferentially suppressed at the STO/LNO interfaces, locally opening a gap as observed in ultrathin LNO films [22].

The physical origin of this effect remains under investigation: Some previous studies have revealed that the MIT in slightly underoxidized LNO films is closely connected to the substitution of Ni³⁺ by Ni²⁺ ions [24,25] leading to a suppression of the electronic states just below the Fermi level. Recently, it has also been proposed that tensile strain at LNO/STO interfaces can drastically enhance the tendency to hole doping due to a stabilization of larger ionic radii of the Ni²⁺ ions [26]. Furthermore, a recent theory study stresses the influence of O 2p states on the interfacial properties: It is suggested that a reduced hybridization of Ni e_g and O 2p states at the interface may lead to a lowering of the e_g -like states and thus drive the interface layer into the insulating state [27]. A detailed study of the depth-resolved charge state of the Ni ions could provide information about the correlation of Ni valency and the DOS at the Fermi level. However, in our experiment, the photon energy was not sufficient to reach Ni 2p, and the Ni 3p core level was overlapping with the Ti 3s states; therefore, the data quality was not good enough to be resolved into multiple components.

In summary, we have conducted a standing-wave soft x-ray photoelectron spectroscopy study of an STO/LNO superlattice. By employing the standing-wave method, we have been able to derive different rocking-curve characteristics for three expected components of the multilayer

sample. Comparison to spectra of a single layer of LNO showed a less-pronounced density of states near the Fermi level, as compared to a thicker LNO film. A detailed analysis of the valence band region revealed a nonuniform electronic structure inside the LNO films with a strong suppression of the Ni e_g and t_{2g} states near the interface to the STO layers that extends over one unit cell. We suggest this interfacial suppression of charge carriers to be the origin of the MIT observed in thin LNO films. Further measurements and calculations will show if this effect is also present at other oxide interfaces and at LNO surfaces. In particular, experiments at higher photon energies or with pairs of layers that do not contain Ti may be used to study a correlation of the Ni valency and the observed opening of a gap at the interfaces.

We are grateful to Leon Balents for helpful discussion and comments. This work was supported by a MURI program of the Army Research Office (Grant No. W911-NF-09-1-0398). The Advanced Light Source and J. B. K. are supported by the Director, Office of Science, Office of Basic Energy Sciences, Materials Sciences and Engineering Division, of the U.S. Department of Energy under Contract No. DE-AC02-05CH11231.

- [1] A. Ohtomo and H. Y. Hwang, *Nature (London)* **427**, 423 (2004).
- [2] J. Mannhart and D. G. Schlom, *Science* **327**, 1607 (2010).
- [3] R. Eguchi *et al.*, *Phys. Rev. B* **79**, 115122 (2009).
- [4] R. Scherwitzl *et al.*, *Appl. Phys. Lett.* **95**, 222114 (2009).
- [5] J. Son *et al.*, *Appl. Phys. Lett.* **96**, 062114 (2010).
- [6] J. Son *et al.*, *Appl. Phys. Lett.* **97**, 202109 (2010).
- [7] J. Chaloupka and G. Khaliullin, *Phys. Rev. Lett.* **100**, 016404 (2008).
- [8] P. Hansmann *et al.*, *Phys. Rev. Lett.* **103**, 016401 (2009).
- [9] S.-H. Yang *et al.*, *J. Appl. Phys.* **103**, 07C519 (2008).
- [10] A. X. Gray *et al.*, *Phys. Rev. B* **82**, 205116 (2010).
- [11] S. H. Yang, A. X. Gray, B. S. Mun, A. M. Kaiser, and C. S. Fadley (to be published).
- [12] W. Smekal *et al.*, *Surf. Interface Anal.* **37**, 1059 (2005).
- [13] J. D. Baniecki *et al.*, *Phys. Rev. B* **78**, 195415 (2008).
- [14] B. Jalan *et al.*, *J. Vac. Sci. Technol. A* **27**, 1365 (2009).
- [15] D. A. Shirley, *Phys. Rev. B* **5**, 4709 (1972).
- [16] L. Henke *et al.*, *At. Data Nucl. Data Tables* **54**, 181 (1993).
- [17] R. M. Feenstra *et al.*, *Phys. Rev. Lett.* **72**, 2749 (1994).
- [18] S. Döring *et al.*, *Phys. Rev. B* **83**, 165444 (2011).
- [19] S. Tanuma *et al.*, *Surf. Interface Anal.* **43**, 689 (2011).
- [20] J. P. Kemp and P. A. Cox, *Solid State Commun.* **75**, 731 (1990).
- [21] K. Horiba *et al.*, *Phys. Rev. B* **76**, 155104 (2007).
- [22] A. X. Gray *et al.*, *Phys. Rev. B* **84**, 075104 (2011).
- [23] P. Pertosa and F. M. Michel-Calendini, *Phys. Rev. B* **17**, 2011 (1978).
- [24] M. Abbate *et al.*, *Phys. Rev. B* **65**, 155101 (2002).
- [25] L. Qiao and X. Bi, *Europhys. Lett.* **93**, 57002 (2011).
- [26] J. Chakhalian *et al.*, arXiv:1008.1373.
- [27] S.-B. Lee *et al.*, arXiv:1107.0724.